Adsorption Equilibrium Constants of Methyl Oleate and Methyl Linoleate in Vapor Phase on Supported Copper and Nickel Catalysts

J.-O. LIDEFELT, Department of Chemical Reaction Engineering, Chalmers University of Technology, S-412 96 Göteborg, Sweden

ABSTRACT

Adsorption equilibrium constants for methyl oleate and methyl linoleate in vapor phase on supported copper and nickel catalysts have been determined using the technique of pulse gas chromatography. The results are discussed in relation to selectivity in fat hydrogenation.

INTRODUCTION

Kinetic studies in heterogeneous catalysis involve theoretical derivations of rate laws expressing reaction rates as a function of temperature and concentrations. The models will contain several parameters such as rate and equilibrium constants of adsorption, desorption, and surface reaction, which normally will be determined by regression methods. If the number of parameters is large, it is often very difficult to discriminate between several physically sound rate laws, which may fit the experimental data equally well. The numerical values of rate and equilibrium constants will normally differ from one model to another. Discrimination may then be feasible if independent data on, for instance, adsorption properties are available.

For parallel and consecutive reactions, it is sometimes possible to explain the selective action of a catalyst by a preferential adsorption of one compound. In fat hydrogenation it is generally accepted that linoleic acid is more readily adsorbed on nickel catalysts than is oleic acid. The surface coverage of linoleic acid will then be much higher than that of oleic acid and, consequently, hydrogenation of dienoic acids will proceed more rapidly than hydrogenation of monoenoic acids.

This paper deals with the experimental determination of adsorption equilibrium constants of oleic and linoleic acid methyl esters on supported copper and nickel catalysts and is part of a study on the kinetics of hydrogenation of fatty acid methyl esters in the vapor phase.

Previous Work

In recent years, much work has been published on adsorption properties of light hydrocarbons (1) and permanent gases (1, 2). However, the amount of work published on adsorption of heavier compounds is very limited. Denisov and coworkers (3) performed work function measurements to determine the heats of adsorption of cyclopentane, cyclopentene, and cyclopentadiene on Pd and Ni films. Adsorption of benzene and cyclohexane on Ni and NiO was studied by Babernics et al. (4). Adsorption data on fatty acid methyl esters or similar compounds have not been reported in the literature.

METHODS

In 1965, Kubin (5, 6) and Kucera (7) developed the theory of pulse gas chromatography. The experimental system consists of a packed bed of porous adsorbent through which inert gas is flowing. A small pulse of adsorbate is added to the inlet stream and the outlet response is monitored as a function of time. Mathematical modeling of this system reveals that the response curve can be interpreted in terms of an axial dispersion coefficient, an external mass transfer coefficient, an effective diffusivity, and adsorption equilibrium and rate constants. During the last ten years, the Kubin-Kucera method has been used by several investigators to determine adsorption and mass transfer properties (8–10). Wiedemann et al. (11) and Schneider et al. (12) found excellent agreement between adsorption equilibrium constants obtained from pulse gas chromatography measurements and values obtained from other methods.

Mathematical Model

Flow in a packed bed with porous adsorbent can be described by three mass balances. If radial symmetry is assumed, the equation governing the bulk flow may be written

$$D_{ea}\frac{\partial^2 c}{\partial z^2} - u\frac{\partial c}{\partial z} - \frac{1-\epsilon_B}{\epsilon_B}\cdot\frac{3\,D_e}{R}\cdot\frac{\partial c_i}{\partial \xi}\bigg|_{\xi=R} = \frac{\partial c}{\partial t} \qquad [1]$$

A symbol list is given at the beginning of the paper.

Mass transfer within a spherical porous particle is described by Equation 2.

$$\frac{D_e}{\epsilon_p}\left[\frac{\partial^2 c_i}{\partial \xi^2} + \frac{2}{\xi}\frac{\partial c_i}{\partial \xi}\right] = \frac{\rho_p}{\epsilon_p}\frac{\partial c_a}{\partial t} + \frac{\partial c_i}{\partial t} \qquad [2]$$

The mass balance of an adsorbed compound is given by

Notation: A, column cross-section, m^2; a_n,b_n, nth Fourier coefficients; c, concentration of adsorbate in bulk flow, mol/m^3; $c^* = c/\int_0^\infty c\,dt$, normalized concentration of adsorbate in bulk flow; c_i, concentration of adsorbate in catalyst pores, mol/m^3; c_a, concentration of adsorbate on catalyst surface, mol/kg; c_{TOT}, active area of catalyst as measured by hydrogen adsorption, mol/kg; D_e, effective diffusion coefficient of adsorbate in catalyst, m^2/s; D_{ea}, axial dispersion coefficient based on void cross-section, m^2/s; h_n, nth coefficient in Hermite polynomial expansion; H_n, nth Hermite polynomial; ΔH_A, adsorption enthalpy, kJ/mol; ΔH_{vap}, heat of vaporization, kJ/mol; k_a, adsorption rate constant, $m^3/kg\,s$; K_A, adsorption equilibrium constant, m^3/kg; K_0, preexponential factor defined in Eqn. 8, m^3/kg; k_f, mass transfer coefficient, m/s; L, bed length, m; q, flow rate, m^3/s; R, particle radius, m; R_g, gas constant; t, time, s; T, temperature, K; T_F, period of Fourier expansion, s; u = q/A, linear velocity, m/s; z, length coordinate in packed column, m. Greek symbols: $\delta(t)$, Dirac delta function; ϵ_B, void fraction of bed; ϵ_p, particle void fraction, ρ_p, particle density, kg/m^3; ξ, radial coordinate in particle, m; μ_1', first absolute moment, μ_2, second central moment.

TABLE I

Initial and Boundary Conditions for the Kubin-Kucera Model

$D_e\left(\frac{\partial c_i}{\partial \xi}\right)\Big\|_{\xi=R} = k_f\left[c(z,t) - c_i(R,z,t)\right]$	external mass transfer
$c < \infty$	if $z \neq 0$
$c_i < \infty$	if $z \neq 0$
$c_i \rightarrow 0$	if $t \rightarrow \pm\infty$
$c_a \rightarrow 0$	if $t \rightarrow \pm\infty$
$c \rightarrow 0$	if $t \rightarrow \pm\infty$
$c(0,t) = \delta(0)$	(Dirac delta function)

Equation 3. In Equation 3, we have assumed a linear adsorption isotherm. If surface coverage is kept very low, this assumption is justified.

$$k_a\left[c_i - \frac{c_a}{K_A}\right] = \frac{\partial c_a}{\partial t} \qquad [3]$$

Initial and boundary conditions are summarized in Table I.

Solving Equations 1-3 for c(t,L) and fitting the theoretical expression to the experimental response curve give the appropriate values of the parameters D_{ea}, k_f, D_e, k_a and K_A. However, an analytical solution of this complex system of partial differential equations cannot be obtained. Kubin (5,6) and Kucera (7) showed that Laplace transformation of Equations 1-3 yields a system of ordinary differential equations which can be solved analytically in the Laplace domain. The inverse transformation cannot be carried out but the expansion in Hermite polynomials finally gives the time domain solution (7).

$$c^*(t,L) = \sum_{n=0}^{\infty} h_n H_n\left[\frac{t-\mu_1'}{\sqrt{2\mu_2}}\right] \exp\left[-\frac{(t-\mu_1')^2}{2\mu_2}\right] \qquad [4]$$

A more convenient way of solving the problem is described by Gangwall et al. (13). They used Fourier transformation and obtained a time domain Fourier expansion of the response curve, which is more readily applicable for computer use.

$$c^*(t,L) = \sum_{n=1}^{\infty} a_n \sin\frac{n\pi t}{T_F} + \sum_{n=0}^{\infty} b_n \cos\frac{n\pi t}{T_F} \qquad [5]$$

where

$$a_n = f_1\,(D_{ea}, k_f, D_e, K_A, k_a) \qquad [6]$$

$$b_n = f_2\,(D_{ea}, k_f, D_e, K_A, k_a) \qquad [7]$$

The parameters in Equations 6 and 7 characterize four different processes taking place in the catalyst column. D_{ea} accounts for axial mixing in the bulk flow, k_f is determined by the magnitude of external mass transfer. Diffusion in the pores of the catalyst is described by the effective diffusivity, D_e, and finally, adsorption by the rate constant k_a and equilibrium constant K_A. All these processes occur simultaneously and, if properly designed, a single experiment should suffice to determine all parameters. Inspection of the solution of Equations 1-3 reveals that only K_A affects the retention time of an adsorbate pulse, while a change in any other parameter in Equations 6 and 7 will alter the shape of the response curve, but not the retention time. This means that K_A is easily determined, but that in many cases it may be difficult to determine more than one of the remaining parameters. In this work axial dispersion in the columns has been excessive since the columns were made very short in order to avoid too long retention times and too much broadening of the pulses. Therefore, within a reasonable range of values, the influence of k_a, k_f, and D_e on the predicted c(t,L) values was small and consequently they were poorly determined, while D_{ea} and K_A were more accurately determined.

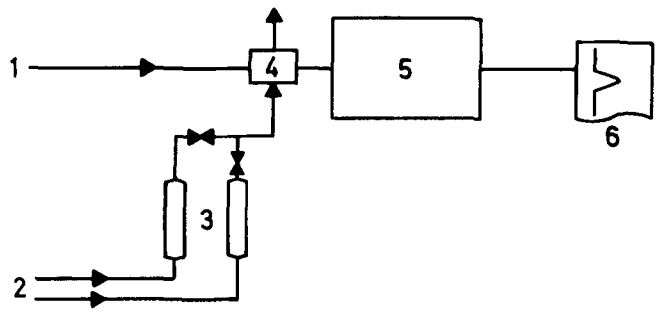

FIG. 1. Schematic flow diagram of the experiment. (1) Carrier gas (N_2); (2) N_2; (3) evaporator; (4) gas sampling valve; (5) GC; (6) chart recorder.

EXPERIMENTAL PROCEDURE

Apparatus

A schematic diagram of the apparatus is given in Figure 1. A conventional gas chromatograph (GC), Carle model 311, equipped with a flame ionization detector was used in the experiments. The GC separation column was replaced by a 1/4 in. SS tube filled with the catalyst, in which adsorption took place. The methyl esters were evaporated into a stream of nitrogen in a packed bed evaporator, held at a constant temperature. The system was equipped with two similar evaporators, one for methyl oleate and the other for linoleate. This facilitates alternation between oleate and linoleate, ensuring that each oleate run has one linoleate run performed under identical conditions with respect to gas flow, temperature, and catalyst activity. Injection of the inlet pulse into the carrier gas stream was facilitated by a gas sampling valve. Outlet pulses were monitored by a chart recorder.

MATERIALS

The catalysts used in this investigation were prepared by an impregnation technique. Cylindrical alpha-alumina pellets were activated in an air stream for 14 hr. After being cooled to room temperature, the pellets were soaked in solutions of copper and nickel nitrate, respectively, for 2 hr. The concentration of metal salt was 0.05 moles per liter. In order to distribute the metal as homogeneously as possible in the pellets, the viscosity of the solution was increased by the addition of 0.5% by weight of methyl cellulose (14).

The excess metal salt on the outer surface was quickly washed off in distilled water and the catalysts were dried and calcinated in air at 500 C for 3 hr. Reduction was carried out in hydrogen atmosphere at 500 C for 3 hr and at 250 C for 3 hr.

The catalysts were ground and sieved before being filled into the column. The fraction kept was between 0.5 and 1.5 mm. In order to obtain a constant activity, the catalysts

TABLE II

Properties of Catalysts and Columns

Catalyst	Ni	Cu
H_2 adsorption (mol H/kg catalyst)	0.86×10^{-3}	0.36×10^{-3}
Metal content (%)	0.1	0.1
Total surface area (m^2/g)	3.5	3.5
Particle diameter (mm)	0.5–1.5	0.5–1.5
Particle porosity	0.45	0.45
Particle density (kg/m^3)	2138	2138
Bed length (mm)	251	60
Column diameter (mm)	4.7	4.7
Bed void fraction	0.52	0.47
Weight of catalyst in column (g)	4.9	1.1

were conditioned by hydrogenation at 220 C for 12 hr before being used in the adsorption experiments.

Metal surface areas were determined by hydrogen adsorption in a static vacuum apparatus. This method is well established for nickel but its suitability for copper surface measurements seems to be disputable. Total metal contents were measured by an atomic absorption spectrometer. Total surface area was determined by adsorption of nitrogen at -196 C. The BET method was used for evaluation of these measurements.

The properties of the catalysts and columns are summarized in Table II.

RESULTS AND DISCUSSION

Experimental conditions and number of runs are summarized in Table III.

TABLE III

Experimental Conditions

	Ni catalyst		Cu catalyst	
	Oleate	Linoleate	Oleate	Linoleate
Temperature range (C)	141–200	148–210	169–216	169–216
Total flow rates (mL/s)	0.4–0.8	0.4–1.3	0.7–1.3	0.7–1.3
Number of runs	18	29	12	14

In Figure 2, the response curves for the two sequential runs are plotted. The difference shown in Figure 2 between oleate and linoleate is more or less pronounced at all experimental conditions and for both catalysts. The front of the oleate curve is steeper, indicating a somewhat slower adsorption. Owing to the uncertainty in the determination of the adsorption rate constant, discussed above, this could not be verified by our calculations. Adsorption equilibrium constants vs inverse temperature curves are given in Figure 3. The heat of adsorption was easily calculated from the van't Hoff equation

$$K_A = K_0 \exp(-\Delta H_A/R_gT) \quad [8]$$

Results of these calculations are given in Table IV. Confidence intervals have been calculated on the 95% level.

The values presented in Table IV indicate that methyl oleate is more strongly bound to the copper catalyst than to nickel, whereas bonding strength for linoleate is equal for nickel and copper.

It is also interesting to note the agreement between the heats of adsorption and heats of vaporization. With one exception (methyl oleate on copper), the difference is less than 25%. Similar results have been obtained for other compounds by other investigators (see Table V). Values of heats of vaporization have been taken from (15). Heats of vaporization for methyl oleate and linoleate were determined from the temperature/vapor pressure relationship at the outlet of the evaporators (saturated mixture) using the equation

$$\text{vapor pressure} \propto \exp(-\Delta H_{vap}/R_gT) \quad [9]$$

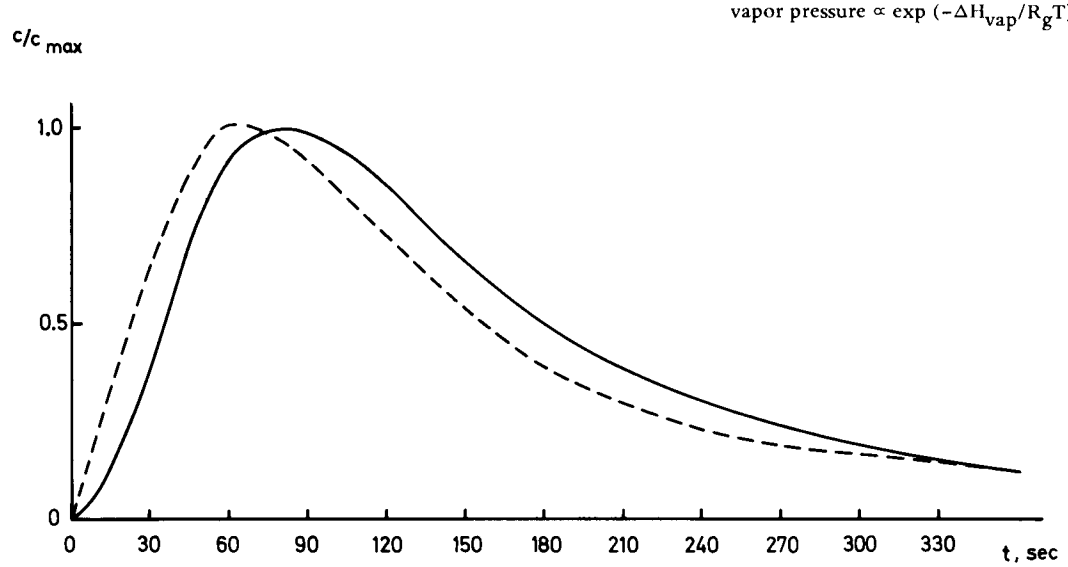

FIG. 2. Pulse response curves for copper catalyst: ——— methyl linoleate; ------- methyl oleate.

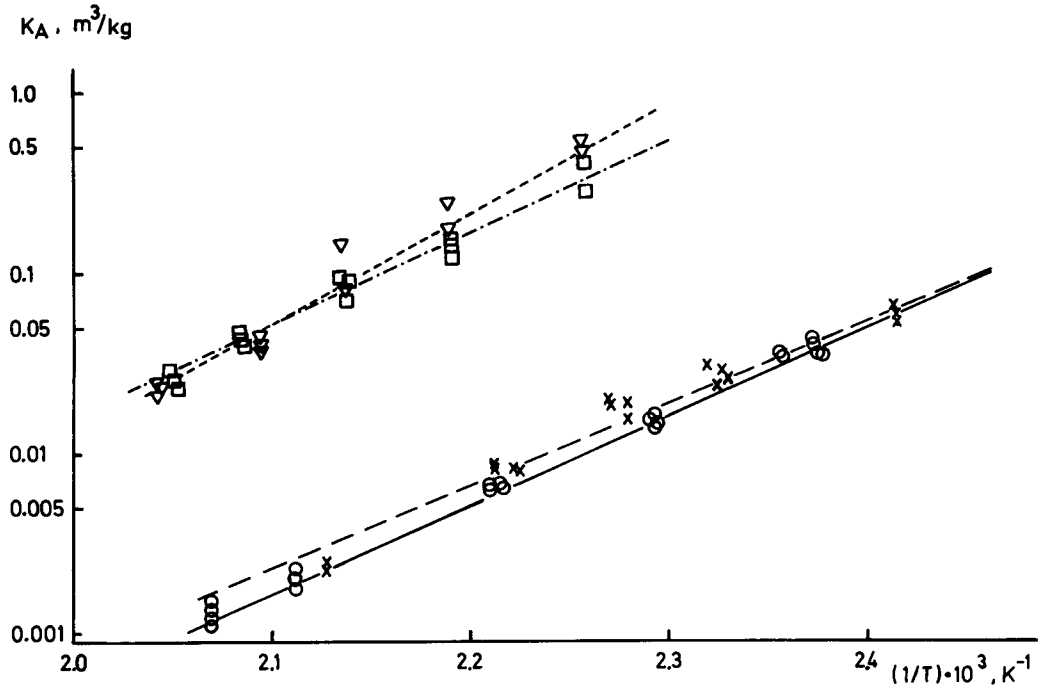

FIG. 3. Plot of adsorption equilibrium constants, K_A, vs inverse temperature.

Nickel catalyst:	oleate	observed x
		predicted ------
	linoleate	observed ○
		predicted ———
Copper catalyst:	oleate	observed ▽
		predicted ------
	linoleate	observed □
		predicted - · - · - ·

When discussing kinetics and selectivity, comparison of adsorption equilibrium constants may be interesting since the magnitude of the equilibrium constants yields information about surface coverages.

A large value of K_A indicates a high surface coverage. In Table VI, K_A has been calculated at three temperatures. The dimension of K_A in Table VI is that adequate for Equations 1-3. The more commonly used dimension bar^{-1} may be arrived at by multiplying with $1/C_{TOT}\ R_gT$.

From Table VI and Figure 3, it may be seen that within the range of temperature of interest there is hardly any difference between the equilibrium constants for oleate and

TABLE IV

Heats of Adsorption

	$-\Delta H_A$(kJ/mol) Cu	Ni
Methyl oleate	115 ± 9	85 ± 6
Methyl linoleate	97 ± 16	94 ± 6

TABLE V

Comparison Between Heats of Adsorption and Heats of Vaporization

Compound	T (C)	$-\Delta H_{VAP}$ kJ/mol	T (C)	$-\Delta H_A$ kJ/mol	Catalyst	Ref.
Cyclopentane	25	28	20-190	12	Pd, Ni	(3)
	50	27				
Cyclohexane	25	33	60-160	21-23	Ni	(4)
	81	30	60-180	26-27	NiO	
Benzene	25	34	160-220	34	Ni	(4)
	81	31	160-220	33	NiO	
Propanol	97	11		7	Silica	(17)
Methyl oleate	150	74[a]	160-200	115	Cu[a]	
				85	Ni[a]	
Methyl linoleate	150	74[a]	160-200	97	Cu[a]	
				94	Ni[a]	

[a]This work.

TABLE VI

Adsorption Equilibrium Constants (m^3/kg Catalyst) for Methyl Oleate and Methyl Linoleate

Temperature (C)	Ni catalyst		Cu catalyst	
	Oleate	Linoleate	Oleate	Linoleate
150	3.7×10^{-2}	3.2×10^{-2}	2.1	1.2
180	7.4×10^{-3}	5.3×10^{-3}	2.4×10^{-1}	1.9×10^{-2}
214	1.5×10^{-3}	9.7×10^{-4}	2.8×10^{-2}	3.1×10^{-2}

linoleate if compared for the same catalyst. Between the copper and nickel catalysts there is, however, a difference of nearly two orders of magnitude. Thus, if we look again at the copper and nickel catalysts separately, surface coverages of oleate and linoleate should be nearly equal, and the difference in rates of hydrogenation for the two compounds may not be attributed to a large difference in surface coverage.

When comparing copper and nickel, the values presented in Table VI indicate a much higher surface coverage of both oleate and linoleate when using copper as hydrogenation catalyst. This may be surprising since it is well known that nickel is far more efficient than copper in catalyzing hydrogenation reactions. More light might be shed upon this problem by investigating the part played by hydrogen. It may also be noted from ΔH_A values in Table IV that oleate is very strongly bound to the copper surface, which may be partly poisoned by oleate, thus lowering catalytic activity. A rough estimation of average lifetimes in the adsorbed state (16) reveals that the mean residence time on the copper surface exceeds that of linoleate by a factor of 100 at 180 C.

Now the question remains whether these results obtained in a gas phase will stand the testing in a real liquid-phase system. This has not yet been done, but in vapor-phase hydrogenations of methyl oleate and linoleate on copper and nickel catalysts, we observed the same kind of selectivity pattern as is known from liquid-phase hydrogenations of methyl esters and vegetable oils.

ACKNOWLEDGMENTS

The Swedish Board for Technical Development provided financial support. The author thanks N.-H. Schöön and J. Magnusson for stimulating discussions.

REFERENCES

1. Hayward, D.O., and B.M.W. Trapnell, Chemisorption, 2nd edn., Butterworths, London, 1964.
2. Toyoshima, I., and G.A. Somorjai, Catal. Rev. 19:105 (1979).
3. Denisov, G.N., V.A. Koljagin, V.D. Jagodovski and V.M. Grjasnov, Kin. Katal. 18:704 (1977).
4. Babernics, L., and P. Tétényi, Z. Phys. Chem. 82:262 (1972).
5. Kubin, M., Coll. Czech. Chem. Commun. 30:1104 (1965).
6. Kubin, M., Ibid. 30:2900 (1965).
7. Kucera, E., J. Chromatogr. 19:237 (1965).
8. Takeuchi, K., and Y. Uraguchi, J. Chem. Eng. Jpn. 10:297 (1977).
9. Scott, D.S., W. Lee and J. Papa, Chem. Eng. Sci. 29:2155 (1974).
10. Wakao, N., K. Tanaka and H. Nagai, Ibid. 31:1109 (1976).
11. Wiedemann, K., A. Roethe, K.H. Radeke and D. Gelbin, Chem. Eng. J. 16:19 (1978).
12. Schneider, P., and J.M. Smith, AIChE J. 14:763 (1968).
13. Gangwal, S.K., R.R. Hudgins, A.W. Bryson and P.L. Silveston, Can. J. Chem. Eng. 49:113 (1971).
14. Kotter, M., and L. Riekert in Studies in Surface Science and Catalysis, vol. 3, Preparation of Catalysts II, edited by B. Delmon, P. Grange, P. Jacobs and G. Poncelet, Elsevier, Amsterdam, 1979, pp. 51-63.
15. Perry, J.H., and C.H. Chilton, (eds.), Chemical Engineers' Handbook, 5th edn., McGraw-Hill, New York, pp. 3-115.
16. Dacey, J.R., Ind. Eng. Chem. 57:26 (1965).
17. Martin, R., J. Cuellar and M.A. Galan, Chem. Eng. Sci. 34:691 (1979).

[Received June 16, 1981]

APPENDIX

SOLUTION OF EQUATIONS 1 AND 3

The Method of Moments

The solution of the set of partial differential equations 1-3 proposed by Kubin (5,6) and Kucera (7), is based on the Laplace transformation. The transformed equations constitute a set of ordinary differential equations which can be solved analytically.

The Laplace domain solution is given by (12)

$$s(z,p) = c_0\ [1-\exp(-pt_1)]\ \exp(-\gamma z) \qquad [A1]$$

where $s(z,p)/p$ is the Laplace transform of the concentration $c(z,t)$ defined by

$$s(z,p)/p = \int_0^\infty c(z,t)\ \exp(-pt)\,dt \qquad [A2]$$

and

$$\gamma = -\frac{u}{2D_{ea}} + \sqrt{\left(\frac{u}{2D_{ea}}\right)^2 + \frac{p}{D_{ea}}[1+h(p)]} \qquad [A3]$$

where $h(p)$ is given by the following expression:

$$h(p) = \frac{3\,k_f}{R}\ \frac{1-\epsilon_B}{\epsilon_B}\cdot \qquad [A4]$$

$$\cdot\left[\frac{1}{p} - \frac{\sin h(R\sqrt{\lambda})}{(p\,D_e/k_f)\sqrt{\lambda}\cos h(R\sqrt{\lambda}) + p\left(1-\frac{D_e}{R\,k_f}\right)\sin h(R\sqrt{\lambda})}\right]$$

where

$$\lambda = \frac{p\,\epsilon_p}{D_e}\left[1 + \frac{(\rho_p/\epsilon_p)\,K_A\,k_a}{K_A\,p + k_a}\right] \qquad [A5]$$

Inversion of the transform is not feasible. However, it is possible to obtain explicit expressions for the moments of the effluent curve from $s(p,z)$.

Using the important properties of the Laplace transform A6-A8 (capital letters denote Laplace transforms),

$$\int_0^t g_1(t)dt = \frac{1}{p}G_1(p) \qquad [A6]$$

$$t^n g_2(t) = (-1)^n \frac{d^n}{dp^n} [G_2(p)] \quad [A7]$$

$$\lim_{t\to\infty} g_3(t) = \lim_{p\to 0} p\, G_3(p) \quad [A8]$$

and the definitions of central moments μ_n and absolute moments m_n of the effluent pulse

$$m_n = \int_0^\infty t^n c(z,t)dt \quad [A9]$$

$$\mu_n = (1/m_0) \int_0^\infty (t-\mu_1')^n c(z,t)dt \quad [A10]$$

where μ_1' is the first absolute moment, one obtains

$$m_n = (-1)^n \lim_{p\to 0} \frac{d^n}{dp^n} [s(z,p)/p] \quad [A11]$$

From equations A1 and A9–A11, the central moments of the curve may be expressed as follows

$$\mu_1' = \frac{L}{u} \left\{ 1 + (1-\epsilon_B)\epsilon_p/\epsilon_B\,(1+\rho_p K_A/\epsilon_p) \right\} + \frac{t_1}{2} \quad [A12]$$

$$\mu_2 = 2L/u \Big\{ (1-\epsilon_B)/\epsilon_B \left[\rho_p K_A^2/k_a + R^2/(3D_e)\,(\epsilon_p+\rho_p K_A)^2 \right.$$

$$\left.(1/5+D_e/Rk_f)\right] + D_{ea}/u^2 \left[1 + (1-\epsilon_B)/\epsilon_B(\epsilon_p + \rho_p K_A)\right]\Big\}^2$$

$$+ t_1^2/12 \quad [A13]$$

Higher moments (cf. 12) are even more complex functions of the parameters K_A, k_a, k_f, D_{ea} and D_e.

The time domain solution c(L,t) may finally be calculated using a Hermite polynomial expansion

$$c^*(t,L) = \sum_{n=0}^{\infty} h_n H_n\left(\frac{t-\mu_1'}{\sqrt{2\mu_2}}\right) \exp\left(-\frac{(t-\mu_1')^2}{2\mu_2}\right) \quad [A14]$$

where $c^*(t,L)$ is the normalized response curve and H_n is the nth Hermite polynomial.

By using the explicit expressions for H_n and the orthogonality of the Hermite polynomials, the coefficients h_n may be expressed through the moments as follows (cf. 13):

$$h_0 = m_0/\sqrt{2\pi\mu_2} \quad [A15]$$

$$h_1 = h_2 = 0 \quad [A16]$$

$$h_3 = \mu_3/[3!\ \sqrt{\pi}\ (2\pi\mu_2)^2] \quad [A17]$$

$$h_4 = (\mu_4 - 3\mu_2^2)/[4!\ \sqrt{\pi}\ (2\mu_2)^{5/2}] \quad [A18]$$

The Fourier Method

Gangwal et al. (13) suggested a solution of Equations A1–A3, based on the Fourier transformations.

The Fourier transform of the normalized output curve

$$c^*(t,L) = \frac{c(t,L)}{\int_0^\infty c(t,L)dt} \quad [A19]$$

is by definition

$$c^*(i\omega) = \int_0^\infty e^{-i\omega t} c^*(t,L)dt = \int_0^{2T_f} e^{-i\omega t} c^*(t,L)dt \quad [A20]$$

where ω is the angular frequency $\omega = n\pi/T_f$ and T_f the period. Separation into real and imaginary parts yields

$$c^*(i\omega) = \int_0^{2T_f} c^*(t,L) \cos\left(\frac{n\pi t}{T_f}\right)dt - i \int_0^{2T_f} c^*(t,L) \cdot \sin\left(\frac{n\pi t}{T_f}\right)dt \quad [A21]$$

Solving the transformed set of equations yields

$$c^*(i\omega) = \exp\left[\frac{uL}{2D_{ea}} - L\sqrt{\sigma}\cos\frac{\psi}{2}\right] \cdot$$

$$\cdot \left[\cos\left(L\sqrt{\sigma}\sin\frac{\psi}{2}\right) - i\sin\left(L\sqrt{\sigma}\sin\frac{\psi}{2}\right)\right] \quad [A22]$$

where

$$\sigma = \sqrt{\alpha^2+\beta^2} \quad [A23]$$

$$\psi = \arctan\left(\frac{\beta}{\alpha}\right) \quad [A24]$$

$$\alpha = \left(\frac{u}{2D_{ea}}\right)^2 + \frac{3k_f(1-\epsilon_B)}{R\,D_{ea}\,\epsilon_B} \cdot$$

$$\cdot\left[1 - \frac{x\cos M \sin h N + y \sin M \cos h N}{x^2+y^2}\right] \quad [A25]$$

$$\beta = \frac{\omega}{D_{ea}} - \frac{3k_f(1-\epsilon_B)}{R\,D_{ea}\,\epsilon_B}\left[\frac{x\sin M\cos h N - y\cos M\sin h N}{x^2+y^2}\right] \quad [A26]$$

x and y are calculated from

$$x = \frac{D_e}{k_f}\sqrt{\gamma}\ \left[\cos\frac{\Theta}{2}\cos M\cos h N - \sin\frac{\Theta}{2}\sin M\sin h N\right] +$$

$$+ \left(1 - \frac{D_e}{R\,k_f}\right)\cos M \sin h N \quad [A27]$$

$$y = \frac{D_e}{k_f}\sqrt{\gamma}\left(\cos\frac{\Theta}{2}\sin M\sin h N + \sin\frac{\Theta}{2}\cos M\cos h N\right) +$$

$$+ \left(1 - \frac{D_e}{R\,k_f}\right)\sin M\cos h N \quad [A28]$$

M and N are given by

$$M = R\sqrt{\gamma}\sin\frac{\Theta}{2} \quad [A29]$$

$$N = R\sqrt{\gamma}\cos\frac{\Theta}{2} \quad [A30]$$

γ is calculated from

$$\gamma = \sqrt{w^2+v^2} \quad [A31]$$

and

$$\Theta = \arctan\left(\frac{v}{w}\right) \quad [A32]$$

where

$$v = \omega\left[\frac{\epsilon_p}{D_e} + \frac{\rho_p K_A k_a^2}{D_e(k_a^2+\omega^2 K_A^2)}\right] \quad [A33]$$

$$w = \frac{\rho_p K_A^2\ \omega^2\ k_a}{D_e(k_a^2+\omega^2 K_A^2)} \quad [A34]$$

The normalized time domain solution c* (t,L) may be expressed as an infinite Fourier series over the interval $0 \leqslant t \leqslant 2T_f$.

$$c^*(t,L) = \sum_{n=1}^{\infty} a_n \sin \frac{n\pi t}{T_f} + \sum_{n=0}^{\infty} b_n \cos \frac{n\pi t}{T_f} \quad [A35]$$

where

$$a_n = \frac{1}{T_f} \int_0^{2T_f} c^*(t,L) \sin \left(\frac{n\pi t}{T_f}\right) dt \quad [A36]$$

and

$$b_0 = \frac{1}{2T_f} \int_0^{2T_f} c^*(t,L)\, dt \quad [A37]$$

$$b_n = \frac{1}{T_f} \int_0^{2T_f} c^*(t,L) \cos \left(\frac{n\pi t}{T_f}\right) dt,\ n > 0 \quad [A38]$$

Combining Equations A21, A22 and A36-A38 finally yields the expressions for the Fourier coefficients a_n and b_n

$$a_n = \frac{1}{T_f} \exp \left[\frac{uL}{2D_{ea}} - L\sqrt{\sigma} \cos \frac{\psi}{2}\right] \cdot \sin \left(L\sqrt{\sigma} \sin \frac{\psi}{2}\right) \quad [A39]$$

$$b_n = \frac{1}{T_f} \exp \left[\frac{uL}{2D_{ea}} - L\sqrt{\sigma} \cos \frac{\psi}{2}\right] \cdot \cos \left(L\sqrt{\sigma} \sin \frac{\psi}{2}\right) \quad [A40]$$